S. James Zinreich, MD • Scot A. Tebo, BS • Donlin M. Long, MD, PhD • Henry Brem, MD
Douglas E. Mattox, MD • Mark E. Loury, MD • Craig A. Vander Kolk, MD • Wayne M. Koch, MD
David W. Kennedy, MD • R. Nick Bryan, MD, PhD

Frameless Stereotaxic Integration of CT Imaging Data: Accuracy and Initial Applications[1]

To evaluate the spatial accuracy of a rapid interactive method of transferring computed tomographic (CT) information between its display on a computer screen to its source (test object, operating field), a multidimensional computer combined with a six-jointed position-sensing mechanical arm was tested with a Plexiglas model consisting of 50 rods of varied height and known location, a plastic replica of the skull, and, subsequently, three patients. The median error value between image and real location was 1–2 mm ($P > .95$), regardless of the registration target sites. The accuracy, however, increased with the selection of widespread registration points, and 95% of all errors were below 3.70 mm ($P > .95$). The results compare favorably with the four most commonly used stereotaxic framed units. A misregistration error of 0.3–2.2 mm was found during intraoperative correlation between anatomy on the CT display and actual anatomic location in the operative field.

Index terms: Computed tomography (CT), three-dimensional, 10.12117, 20.12117 • Computers, examination control • Skull, abnormalities, 10.1439 • Skull, neoplasms, 125.3641, 239.373 • Stereotaxis, 10.1299, 20.1299

Radiology 1993; 188:735–742

[1] From the Departments of Neuroradiology (S.J.Z., S.A.T., R.N.B.), Neurosurgery (D.M.L., H.B.), Otolaryngology–Head and Neck Surgery (D.E.M., M.E.L., W.M.K.), and Maxillofacial Reconstructive Surgery (C.A.V.K.), The Johns Hopkins Medical Institutions, Meyer 8-140, Baltimore, MD 21205; and the Department of Otorhinolaryngology–Head and Neck Surgery, University of Pennsylvania, Philadelphia (D.W.K.). Received April 7, 1992; revision requested May 29; final revision received May 12, 1993; accepted May 13. **Address reprint requests to** S.J.Z.

In the past 2 decades advances in the radiologic and laboratory diagnosis of neoplasms, together with advances in surgical and adjunctive therapy, have improved the outcome of patients with many intracranial and head and neck tumors. The early diagnosis of tumors, the accurate image delineation of their size and location, and subsequent complete surgical removal are factors that have most influenced patient survival (1–3). Radiographic information is typically used to identify the location, extent, and size of pathologic entities. The subsequent surgical removal of these tumors, however, remains primarily an exercise in psychomotor eye-hand coordination, with the surgeon intuitively transferring radiographic information to the surgical site. Limited surgical fields of view and indistinct margins between normal and pathologic tissue often restrict accurate intraoperative determination of tumor boundaries (4). Neurosurgeons are especially hampered because of limited ability to visually distinguish among tumor tissue, peritumoral edema, and normal brain parenchyma (5). This limitation at least partially accounts for the relatively high incidence of incomplete tumor excision, recurrence, and the need for reoperation. The surgeon's success is dependent on the accurate mental transfer of computed tomographic (CT) and magnetic resonance (MR) imaging information to the operative site to assist direct visual perception of tumor.

CT- and MR imaging–adapted stereotaxis and intraoperative ultrasonography (US) techniques are currently used to improve this intuitive process. Even though the stereotaxic frames attached to the patient's head aid in the precise localization of a tumor, frames can hinder access to and exposure of the surgical field, especially for tumors in the posterior fossa and skull base. These frames can also cause substantial discomfort and inconvenience to the patient. Changes in tissue characteristics during surgery limit the ability of US to accurately depict the margins of many tumors (6).

In an attempt to address these issues, computer hardware and software were developed to reconstruct two-dimensional digital images into a three-dimensional (3D) volumetric image display. This reconstruction provides a display that the surgeon can use not only to diagnose but also to actively guide the surgical procedure (7,8). The 3D images, when combined with a mechanical sensor probe, can be directly spatially registered to the structures in the surgical field. The probe position can then be guided by means of the display, thus eliminating the guesswork of intuitive transfer of radiographic information to the operative field. This 3D computer-based robotic device provides an objective and accurate integration of imaging data with the structures in the operative field (9). Even though the system is a stereotaxic technique in principle, its greater operative flexibility compared with that of a conventional frame system can be a decided advantage in many situations. The use of such equipment is obviously dependent on the accuracy and reliability with which it can correlate the location of structures in the operative field with the corresponding representation of the structure on the two-dimensional or 3D image on the computer screen. The purpose of this work is to evaluate the accuracy and reproducibility of this computer image–assisted surgical equipment and to describe its initial application in three patients.

MATERIALS AND METHODS

Stereotaxic System

The stereotaxic software was created by I.S.G. Technologies (Mississauga, Ontario,

Abbreviation: 3D = three-dimensional.

Canada) and is currently implemented with an IRIS 4D workstation (Silicon Graphics, Mountain View, Calif). In addition to the on-board processors, the system uses a separate set of display processing boards created by I.S.G. Technologies for use in their Allegro 3D reconstruction workstation.

The workstation is interfaced with the Surgicom (Faro Medical Technologies, Lake Mary, Fla), a passive, articulated mechanical arm that is used to perform the stereotaxic spatial measurements. The arm was constructed with 2 degrees of freedom at each of the three joints. A metallic endoscopelike probe is attached to the arm at the last joint. Sensors at each of the six rotational axes pass information about the relative angles of the arm segments to the computer by means of an analog-to-digital conversion board. These data are used in conjunction with known geometric information about the arm and the probe to trigonometrically solve for the spatial position and orientation of the device. The probe tip is used as the point of interest for stereotaxic location.

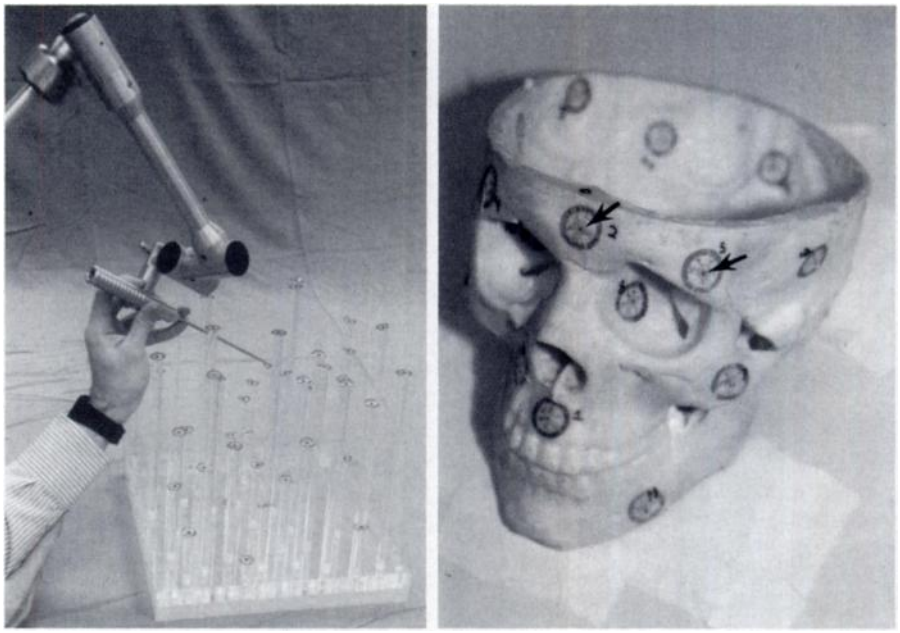

a. b.

Figure 1. **(a)** Plexiglas phantom. Fifty Plexiglas rods of known height were implanted at known locations in a base unit. **(b)** Plastic skull. Three-millimeter lead pellets (arrows) randomly taped to the calvarial and maxillofacial surface were used as markers to test the "locator" accuracy of the probe tip.

Registration

The registration process conveys to the computer (containing the 3D representation of the object to be evaluated) the precise location and orientation of the object, such that the image of the probe tip on the computer screen shows the actual position of the probe tip on or in the object. As each registration marker on the object is touched with the tip of the probe, the corresponding marker's representation on the computer image is identified by a mouse-driven cursor on the screen. This results in a point pair file that contains the real space and image space locations of each of the markers. By using rigid body translational and rotational motions, a least-squares fit is performed between these groups of corresponding point pairs, resulting in a linear transformation matrix that is used to align the computer data with the subject. The root mean square error obtained from the least-squares fit is reported to the operator as an indication of the registration accuracy. A visual check of the registration is made by touching widely separated anatomic points on the surface of the patient's head and confirming the indicated locations on the computer screen.

Data Presentation

Once the registration has been accomplished, the stereotaxic data can be displayed on the computer screen in a number of ways. A 3D probe image can be displayed on the screen along with the reconstructed data. This model represents the actual position and orientation of the real probe in relation to the patient's head. As the probe is advanced, the reconstructed object or objects are cut away in three orthogonal planes intersecting at a single voxel that represents the current location of the probe tip. For reasons of visibility, the probe image is displayed with a blunt tip on the computer screen.

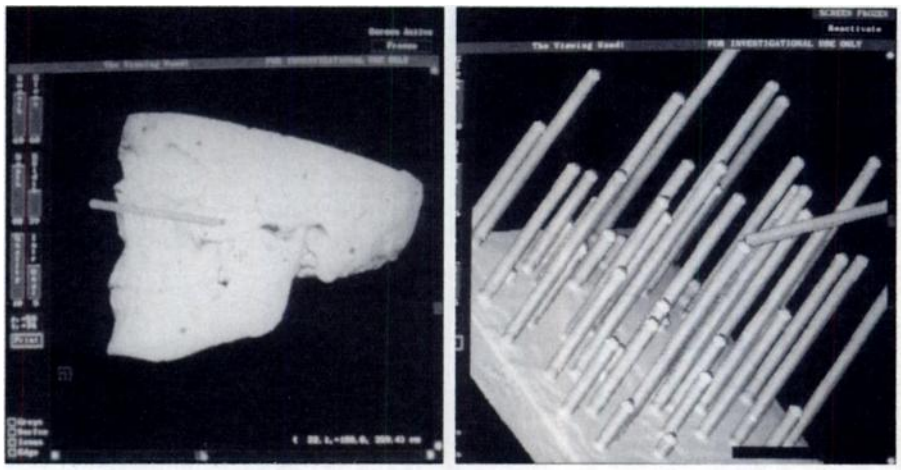

a. b.

Figure 2. Three-dimensional reconstructions of **(a)** the plastic skull and **(b)** the Plexiglas phantom.

The data can also be displayed as three orthogonal cuts through the original 3D CT data. In this mode, cross hairs represent the position of the probe tip on axial, coronal, and sagittal views (two of the views being reconstructed from the original data). In addition, an oblique projection can also be displayed along the trajectory of the probe. Again, the position of the probe tip is represented by cross hairs.

Scanning Parameters

Standard CT scanning parameters suffice for 3D data collection, with only a few additional considerations. To provide adequate out-of-plane resolution for the 3D reconstructed objects and the two-dimensional reconstructed views, the section thickness must be smaller than that typically used for diagnostic scans. Also, to provide a proper 3D data set, adjacent sections must be contiguous, meaning that the table position increments must be equal to or smaller than the section thicknesses. Clinical experience has led us to use a standard protocol of 4-mm section thicknesses with 3-mm table incrementation. Attention must also be paid to the placement of the registration fiducial markers to ensure that the section stack encompasses the entire marker set. Because of marker placement considerations, this means that the section stack will usually be larger than that of ordinary clinical scans.

a.

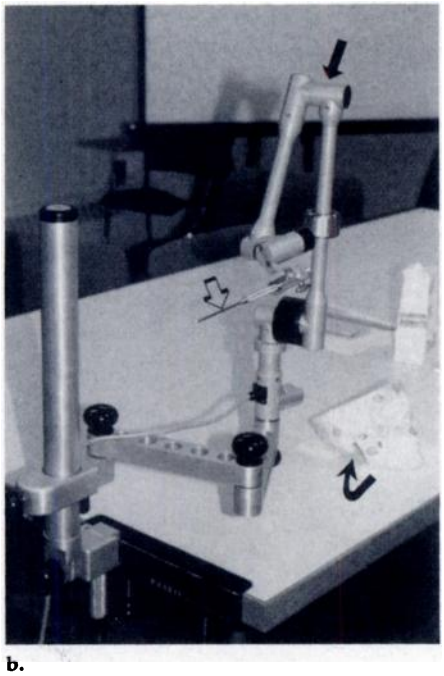

b.

Figure 3. Equipment. **(a)** Computer (C), the display screen with a 3D display of the test subject and attached markers (solid arrow), mouse (open arrow), and a video image integrator (✱) on a mobile cart. **(b)** The six-jointed mechanical arm (solid straight arrow) is attached to the side of a table and holds an endoscope replica (open arrow). The test object (curved arrow) is taped to the table in easy reach of the arm.

The restrictions on scanning parameters make it necessary in most cases to obtain a data set specifically for use with the stereotaxic system. Standard clinical scans are usually not sufficient for the purpose, although if candidates for stereotaxic procedures are identified early enough, the 3D protocol can be implemented for the initial scans.

In Vitro Evaluation

Two different models were used to establish the accuracy of the system. The first of these consisted of a rigid base in which 50 Plexiglas rods were implanted (Fig 1a). The phantom was constructed such that the locations and heights of the rods were known, giving well-defined stereotaxic coordinates for the tip of each rod. The rods were placed in such a manner as to scatter the stereotaxic points throughout a volume of approximately 25 cm^3, a fair approximation to the volume of the head.

A plastic replica of the skull, including structures, served as our second experimental model (Fig 1b). Thirty-three metallic markers (3 mm in diameter) were randomly taped to the surface of the maxillofacial region, outer surface of the calvarium, and inner surface of the base of the calvarium to obtain a pseudo-uniform distribution over these surfaces. These markers, the same as those routinely used for clinical patients, were used to perform the image-phantom registration and to establish the registration accuracy of the system.

The Plexiglas phantom and the plastic skull, with markers in position, were scanned in the axial position with a Somatom DR 3 scanner (Siemens Medical Instrumentation, Iselin, NJ) by using 4-mm section thickness, 3-mm table incrementation, 125 kVp, 450 mAs, and 4-second scanning time. The CT image data were transferred by means of a nine-track magnetic tape to the workstation. By using a thresholding, seed growing, and boundary recognition software program, the initial CT data were three-dimensionally reconstructed into objects representing the base and rods in the case of the Plexiglas phantom and the markers and maxillofacial-calvarial outline in the case of the plastic skull (Fig 2). The 3D reconstructed objects, along with the original section data, were transferred to the stereotaxic workstation (Fig 3a).

The mechanical arm was clamped to a table in a manner similar to that used in the operating room. In intraoperative use, the patient's head would be fixed in place by a Mayfield head holder or other similar device. Since this was impractical for the phantom, the plastic skull was immobilized (taped to the table) near the mechanical arm (Fig 3b). The Plexiglas phantom was secured in a like manner.

The tips of six of the rods around the periphery of the Plexiglas phantom were chosen for registration. A different set of rods was chosen for each trial. A total of five registrations and subsequent measurements were performed.

Five separate subsets of markers, consisting of six markers each, were used for registration with the plastic skull. These subsets are identified by their regional location: the anterior, right, and left lateral surfaces of the face, the occipital cranial surface, and scattered locations around the entire calvarium (global). Registration was performed five times with each of the five registration sets.

Accuracy Measurement

The tip of the probe was touched to the end of each of the 50 rods making up the Plexiglas phantom. The image space location of the probe tip, as derived by means of the transformation matrix, was recorded. The actual locations of the tips of the rods, as measured with a ruler, were also entered into the computer. A least-squares fit of the two data sets was performed to translate them into the same frame of reference. The distance, in millimeters, between corresponding points in the two data sets was calculated by using the Pythagorean theorem.

Each of the 33 markers taped to the plastic skull, including the markers used for registration, were sequentially touched with the tip of the probe. Simultaneously, the center of the cursor (cross hair) on the computer screen was placed on the 3D reconstruction of the same marker. By using the transformation matrix obtained during registration, the graphic space position of the probe tip was computed and recorded, along with the coordinates of the reconstructed marker as indicated by the cursor. The computer then calculated the difference between the two positions in millimeters.

The five subsets of markers were located in different areas of the calvarium to test the accuracy of the system as a function of the location of the registration set. Each registration was performed five times to test reproducibility and to provide a broader base for statistical measurements.

Patient Studies

Three patients were used to demonstrate the clinical accuracy of the system. Each patient was evaluated with a CT examination after placement of five markers on the scalp, face, or both close to the operative site. These markers were the same as those used on the plastic skull. The scanning parameters were identical to those used to evaluate the plastic skull. After the CT data were transferred to the computer, a 3D reconstruction of the markers, skin, maxillofacial area and calvarium, intra- and/or extracranial pathologic features, and relevant intracranial structures was performed. Each structure was defined as a volume of interest and was highlighted with one of several colors offered by the computer software. The data were then transferred to the stereotaxic workstation. The computer system, including its 3D data, display screen, and the mechanical arm, was moved to the operating room. The patients were routinely immobilized in a Mayfield head holder, and the mechanical arm was attached to the operating table close to the head so that the probe tip could easily reach the operative site. The markers that had been left on the scalp or face were used for registration.

After registration, an operative sterile field was established. The probe was detached from the mechanical arm and steam sterilized. A sterile plastic drape was placed on the mechanical arm. After the probe was sterilized, it was reattached to the sterilely draped mechanical arm. At this point the system was ready to be used by the surgeon to display the relationships of subcutaneous or intracranial pathologic conditions to skin surface, outline site and extent of skin incision, osteotomy site, and location of tumor, as well as various bone

and soft-tissue landmarks. The accuracy of localizing various anatomic structures and surgical landmarks was then determined (Fig 4). Because the intent was to demonstrate the accuracy of the system, cases with easily visible and identifiable landmarks were chosen for inclusion in the study. In clinical use, the real value of the system could be in localizing objects that are not as readily found.

RESULTS

Experimental Model

Five trials were performed with the Plexiglas phantom, involving 50 independent measurements each, for a total of 250 measurements. The results are presented in Table 1.

Five trials involving 31 independent measurements were performed for each of five different registration sets for the plastic skull, producing a total of 775 measurements. Two markers on the mandible were not included in the data analysis because of an inadvertent displacement of the markers by movement of the mandible after scanning. The results are presented in the histogram error distribution graphs (Fig 5) and the probability interval graphs (Fig 6) for each registration set (facial, left and right lateral, back, and global) and for a composite data set made up of all of the measurements from each set. A correlation analysis between accuracy and the distance of markers to the registration sets was also performed, but there was only a weak relationship between the two.

The median, mean, standard deviation, 95th percentile value, maximal value, upper bound of the two-sided 95% confidence interval for the median, and upper bound of the one-sided 95% confidence interval for the 95th percentile for each registration set are summarized in Table 2. The confidence intervals were calculated by using distribution-free quantile order statistics (10).

The histogram plots were constructed by classifying each of the measured errors for the classes indicated into an error range indicated by the bin labels on the x axis. They formed an overall picture of the error distribution. The cumulative distribution functions were created by plotting at each error value the percentage of total error measurements that fell below this number. The plots were created by simply connecting successive points. The apparent smoothness of the plots is due to the large sample size. Thus, by reading across the graph, we can see that 90% of the errors fell below 3 mm. This graph gives us a means by which to estimate the probability that future errors will be within some specified range. We can say, for example, that it is approximately 90% probable that a future measured error will be less than 3 mm.

Table 1
Results of Plexiglas Phantom Trials

Statistical Measure	Measured Error (mm)
Median	1.00
Upper confidence bound ($P > .95$)	1.10
Mean	1.12
Standard deviation	0.61
95th percentile	2.29
Upper confidence bound ($P > .95$)	2.46
Maximal value	3.24

Note.—A total of 250 measurements were performed.

Table 2 presents the error values broken down into registrations sets. It demonstrates that the accuracy of the system is dependent on which registration set is used. Errors for a registration set in which the markers are fairly coplanar, as in the case of the facial registration, are typically higher than those in which the points encompass a larger volume, the global registration set being the prime example. This difference is reflected in the average error measurements.

From these data, it is expected that the average error values will be in the range of 1–2 mm, regardless of registration set. Typical maximal error values are expected to be between 4 and 5 mm, with 95% of the errors occurring in the range between 0 and 3.7 mm.

Patient Case Summaries

Patient 1.—An 8-year-old boy was born with right frontal flattening secondary to right coronal synostosis (plagiocephaly). He already had undergone two previous surgical corrections, but treatment of his craniofacial problem was still incomplete. The current operative procedure consisted of a bifrontal craniotomy and a bilateral orbital advancement to correct the flattened, supraorbital, and lateral orbital rims. This procedure was followed by reshaping and reconstructing the flattened forehead abnormality. The frameless stereotaxic image integrator was helpful in identifying the position of the orbital rims and in evaluating the projected reconstruction in comparison to the uninvolved opposite side. Osteotomies of the frontal bone and superior orbital rim were performed. The right superior orbital rim was advanced forward to establish facial symmetry. The orbital advancement on the right side was 17 mm (measured with calipers), and the computer-guided instrument measured 17.3 mm (Fig 7).

Patient 2.—A 46-year-old man underwent removal of a verrucous carcinoma of the pterygopalatine fossa that extended to the Meckel cavity. The anterior wall of the left maxillary sinus was opened by means of a sublabial incision. A small punctum of tumor was present on the posterior wall of the maxillary sinus at endos-

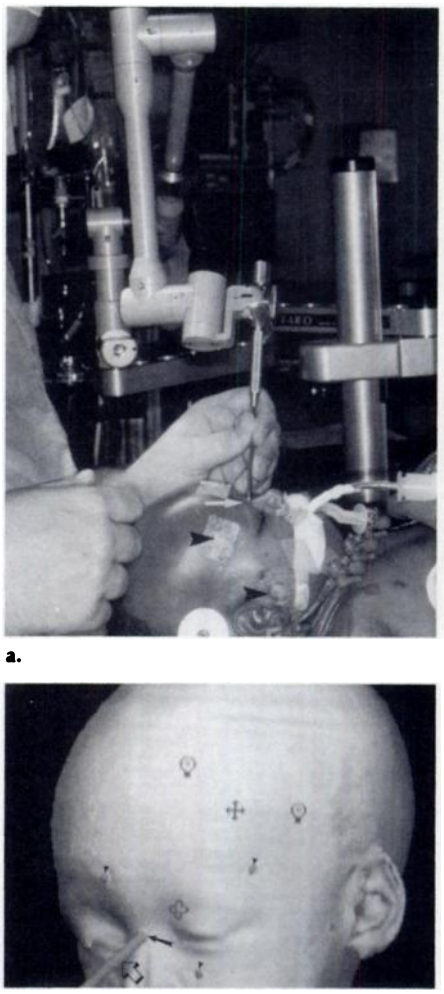

a.

b.

Figure 4. Accuracy verification during craniofacial surgery in an 8-year-old boy. **(a)** Mechanical sensor tip is touching the metal marker on the nasion (arrow). Additional markers are taped to the skin (arrowheads). **(b)** Three-dimensional image of scalp and skin surface overlying the maxillofacial structures shows the position of the distal end of the mechanical sensor (open arrow) covering the marker on the nasion (solid arrow). Additional markers are indicated with arrowheads.

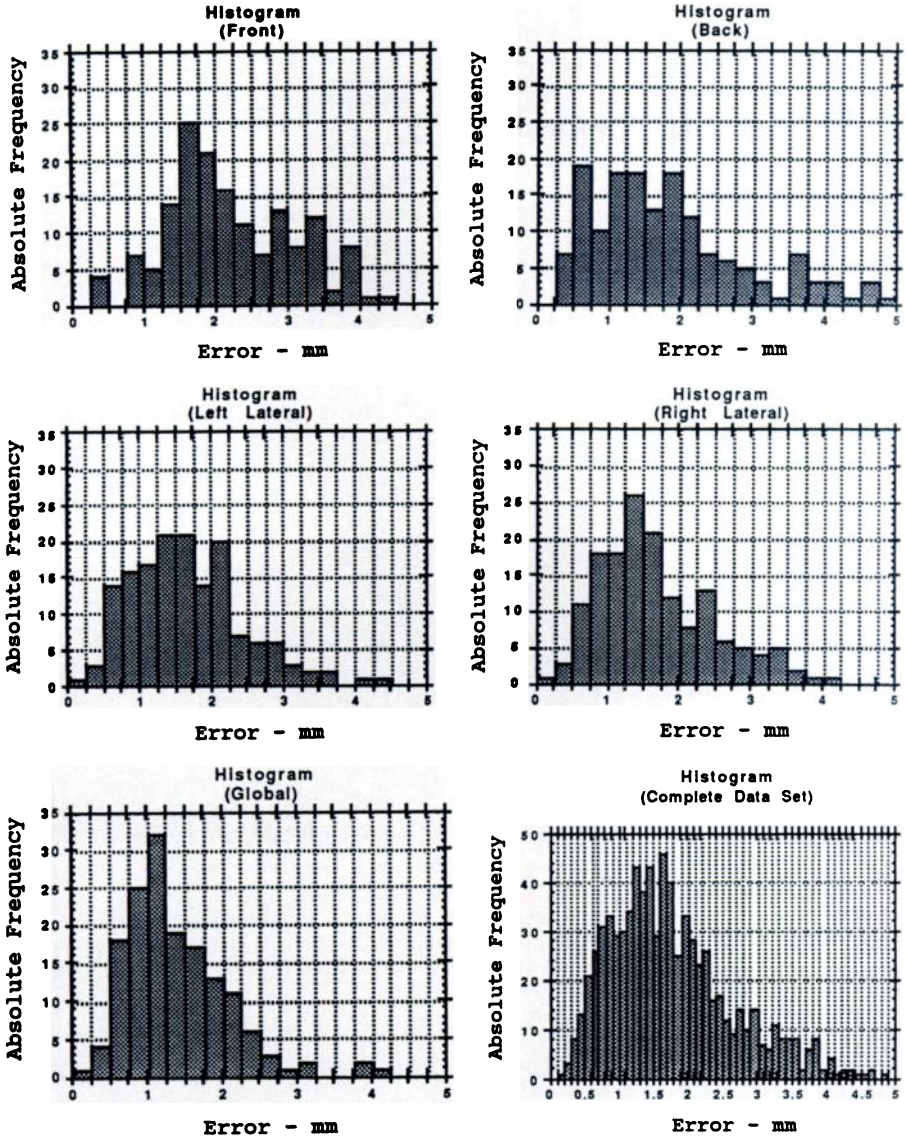

Figure 5. Error values within the specified intervals are placed in respective bins to provide a total count of the number of errors in each range. The graphs show the distribution of errors for each registration set (n = 151) and a composite set made up of the data from all the registration sets (n = 775).

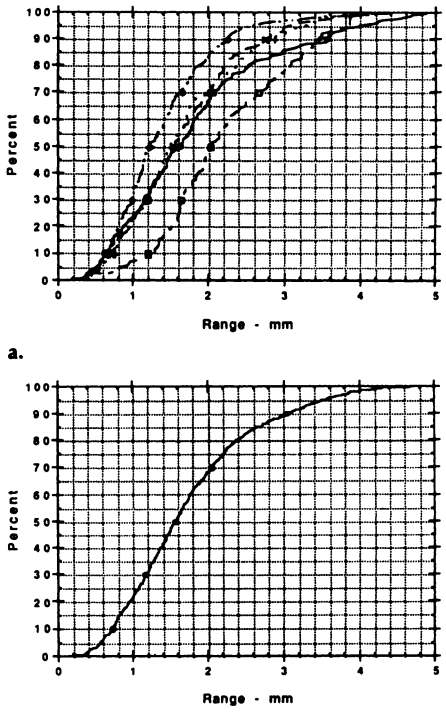

Figure 6. Percentage of the **(a)** individual data sets and **(b)** composite data set falling below the error indicated on the abscissa is plotted, providing an estimation of the probability that future errors will fall below this value. The apparent smoothness is due to the large number of samples (n = 775). In **a**, ○ = back, □ = front, ◇ = global, × = left, and + = right.

copy. This punctum extruded keratinous debris. This punctum was also detected on the CT examination. The computer-guided probe was introduced into the maxillary sinus and placed on the punctum. The positional error of the probe tip on the computer screen versus the reconstructed position of the punctum measured 1.8 mm (Fig 8).

Patient 3.—A 62-year-old woman underwent a mastoidectomy for removal of an acoustic neuroma. During the course of the operation the probe of the frameless computer-guided stereotaxic integrator was positioned adjacent to various anatomic landmarks to establish the accuracy of the integrator in localizing the temporal bone anatomy. Figure 9 shows its accuracy in integrative correlation of the actual temporal bone anatomy in the surgical field, with corresponding anatomy displayed on the 3D image on the computer screen. The calculated error of the probe tip position on the jugular bulb, the tip of the mastoid bone, and the lateral border of the acoustic neuroma on the screen, when compared with the actual probe tip position in the operative field, was 2.2 mm.

DISCUSSION

Conventional stereotaxic surgery involves use of an external framework that, when attached to the patient, affords geometrically determined vectors that can direct the surgical procedure to a specific site (11). Stereotaxic surgery helps in planning the optimal surgical approach and guides the surgeon to deep-seated lesions that may be hidden from view. This instrumentation has been used to ablate seizure foci (12–14), perform biopsies of tumors (15–17), and implant radiation seeds (18–19). The positioning of a stereotaxic frame on a patient, however, requires additional time and training for surgeon and staff, increases patient trauma (and therefore discomfort), and may introduce presurgical and intrasurgical complications (11). Furthermore, the device itself may limit the surgeon's access to the surgical field.

Computers are now available that, when outfitted with a robotlike mechanical arm, as described above, afford stereotaxis with CT (or MR imaging) data but without the need for frames. This system is not attached to the patient and is freely and easily movable around the patient without interfering with the surgical site. Its accuracy is similar to those of four commonly used stereotaxic frame systems (Leksell [Elekta Instruments, Tucker, Ga], BRW and CRW [Radionics, Burlington, Mass], and Kelly-Goerss, which is a modified Todd Wells system [Stereotactic Image Systems, Salt Lake City, Utah]) (Table 3) (11).

It is necessary in any discussion of the application of stereotaxic devices to distinguish between the terms accuracy

and precision. Accuracy may be defined by the success of the device in reaching a known location in space. Precision is the ability of the device to return to the same location in space repeatedly. In the current series of experiments, the accuracy of the device is demonstrated with the trials involving the Plexiglas phantom. In these trials, the position of the tips of the Plexiglas rods was known, having been provided by means of an external reference system, in this case a ruler. This knowledge provided an external framework by which the success of the device in reaching these known points could be measured. The results of these trials, presented in Table 1, show that the frameless system is accurate within approximately a millimeter. The accuracy having been established, the precision of the device can then be ascertained with the trials involving the plastic skull.

Despite the relatively high accuracy of the frameless stereotaxic device, several sources of inherent error should be considered in the effort to achieve optimal quality examination and procedural accuracy.

Table 2
Results of Plastic Skull Trials

Statistical Measure	Measured Error (mm), by Registration Set					
	Facial	Left Lateral	Right Lateral	Back	Global	Combined Data Set
Median	2.02	1.55	1.50	1.62	1.22	1.60
Upper confidence bound ($P > .95$)	2.25	1.73	1.69	1.79	1.40	1.67
Mean	2.21	1.66	1.66	1.81	1.39	1.74
Standard deviation	0.87	0.79	0.80	1.05	0.69	0.89
95th percentile	3.78	3.02	3.26	3.97	2.55	3.55
Upper confidence bound ($P > .95$)	3.87	3.60	3.50	4.51	3.23	3.70
Maximal value	4.31	4.42	4.11	4.88	4.02	4.88

Note.—A total of 775 measurements were performed.

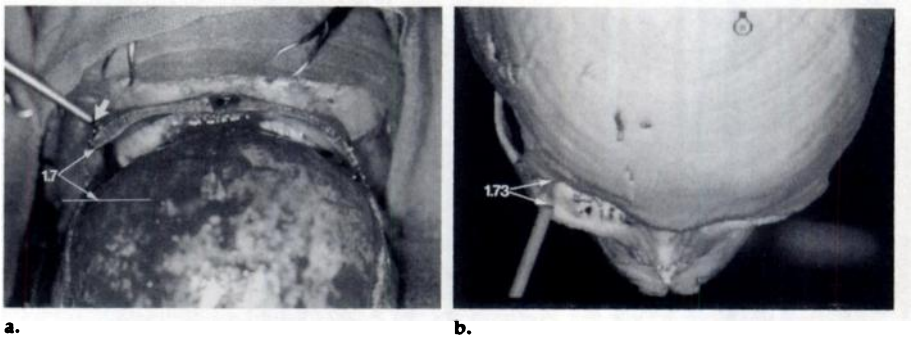

a. b.

Figure 7. Superior orbital rim advancement in an 8-year-old boy. **(a)** The probe tip (arrow) is on the reconstructed orbital-supraorbital bar, 1.7 cm anterior to its previous position (established with calipers) (line). **(b)** Three-dimensional display shows the position of the probe tip in spatial relation to postoperative placement of the orbital bar, which is 1.73 cm from the preoperative position of the supraorbital rim.

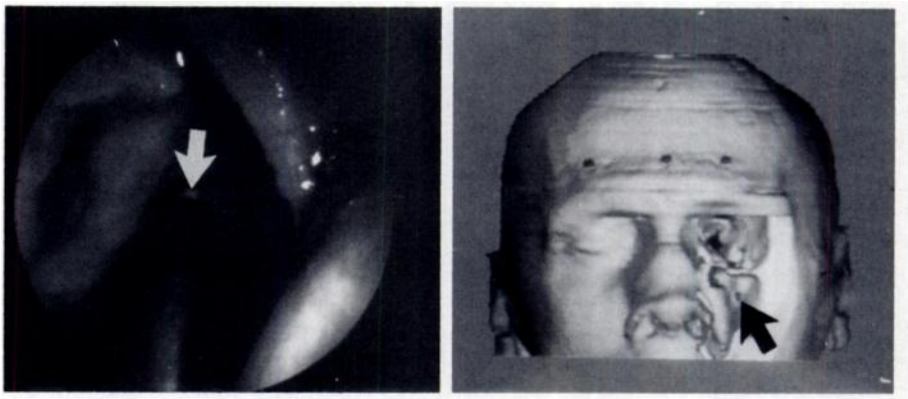

a. b.

Figure 8. Localization of a posterior maxillary sinus wall punctum in a 46-year-old man. **(a)** Probe tip is positioned on the punctum (arrow) with endoscopic guidance. **(b)** Arrow shows probe tip position on 3D display of the maxillary sinus punctum. The calculated error was 1.8 mm.

Source of Error Produced by the Scanning Method

Galloway et al have shown that CT section thickness significantly influences the accuracy of each of the four most commonly used frame stereotaxic systems (11). Accuracy was highest when 1-mm section thicknesses were used, with the mean accuracy ranging from 1.0 to 1.9 mm. In their evaluation, when 4-mm CT section thicknesses were used, the mean accuracy ranged between 2.5 and 3.2 mm. Thus, the thinner the CT sections, the more accurate the procedure. It is obvious that geometric distortions caused by the scanner hardware or software will lead to errors in the acquired data set. Proper scanner maintenance and calibration should minimize this problem. Errors that cannot be compensated for, such as patient movement during scanning and artifacts introduced by foreign objects (spray from the lead marker pellets), may also degrade the information, adversely affecting accuracy. These sources of error would affect the frameless stereotaxic device in a similar way.

Source of Error Produced by the Reconstruction Process

The 3D reconstruction process is based on a thresholding process followed by interpolation in which round-off error and visual approximations occur. A discrepancy between real and reconstructed objects and structures may thus occur. Hildebolt et al (20) concluded that errors in measurements of skull anatomy parameters from 3D reconstructions could range up to 5 mm. Although their methods are not directly applicable to the case in question, we can conclude that errors of this type could affect the stereotaxic system in two different ways.

First, inaccuracies in identifying the position of the fiducial markers during registration could introduce errors in the data fit to the patient. These errors are at least partially offset by the least-squares fitting routine. Second, although the system may be correctly depicting the location of the probe tip, ambiguities in the display of the 3D data on the screen may cause the location to be perceived incorrectly by the viewer. These ambiguities can be re-

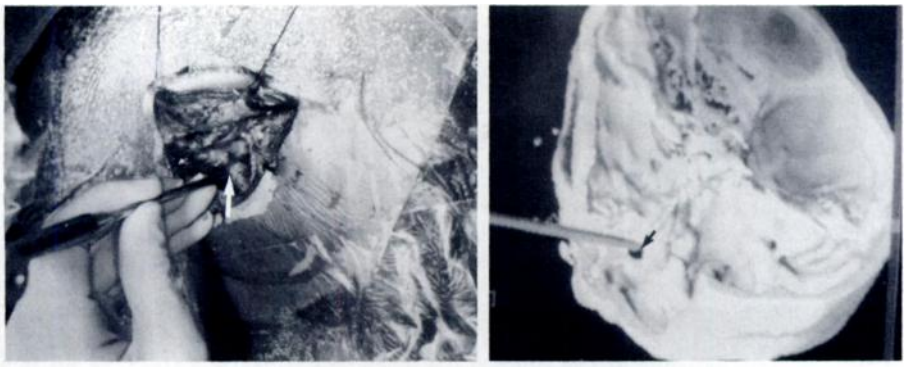

a. b.

Figure 9. Localization of the superolateral surface of a "high" jugular bulb (arrow in **a** and **b**) **(a)** during mastoidectomy and **(b)** on the computer screen. The calculated error of the probe tip position on the screen was 2.2 mm.

Table 3
Comparison of Accuracy of Stereotaxic Systems

Statistical Measure	Error (mm), by System				
	BRW	CRW	Kelly-Goerss	Leksell	I.S.G.-Faro Combined Skull Data Set
Mean	2.7	2.6	2.5	3.2	1.7
Standard deviation	1.3	1.5	1.4	1.3	0.9
Maximum value	7.0	7.1	6.2	5.2	4.9

Note.—Data for BRW, CRW, Kelly-Goerss, and Leksell equipment were adapted from reference 11.

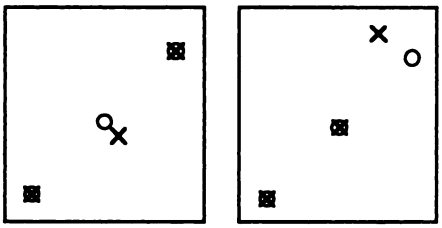

a. b.

Figure 10. Simple illustration of global registration. The error for the misaligned point in **a**, in which the two outermost points are fitted exactly, is less than that in **b**, in which two points at one end were fitted exactly.

duced by the use of the triplanar cross-sectional views. There is obviously room for improvement in data reconstruction and image display and presentation.

Mechanical arm error.—Changes in temperature, aging, and bending of the stereotaxic device, as well as round-off errors in software, may influence the accuracy of any of these devices.

Registration and transformational error.—Inaccuracies may arise from improper positioning of the sensor tip or cursor on the registration marker. In selecting registration points, the exact center of a marker image cannot always be determined. Some disparity may exist between the position pointed to with the probe and the position appearing on the screen. In addition, loose skin may induce marker movement during or after the registration process. To avoid the latter registration errors, markers should be placed on skin with the least mobility. The least-squares fitting registration algorithm tends to average out the error associated with a single point. The registration improves as more points in more places are entered. Movement after registration will naturally invalidate the registration. To avoid errors from patient or arm movement, one might choose to affix the arm to the patient immobilizing frame (Mayfield frame) or add a head-tracking device to the frameless stereotaxic unit.

Mechanical Accuracy versus Application Accuracy

Galloway and Maciunas, in their review of stereotaxic neurosurgery techniques (21), defined the difference between these two terms. In their words,

> *Mechanical accuracy* has to do with the quality of the apparatus construction. What is the average endpoint error relative to a known location across the total motion of the device? *Application accuracy* is the accuracy of the device as it will be used in a real-world setting [during surgery].

In their evaluation of the most widely used framed stereotaxic units, Galloway et al (11) stated that the manufacturers of these devices report mechanical accuracy, which they define in this instance as the end point error, given a half-maximal step error for each degree of freedom inherent to the device. They point out that this results in the lowest possible error measurement because it is independent of imaging parameters. The inclusion of clinically required imaging parameters, they claim, accounts for the two- to six-factor discrepancy between their results and those reported by the manufacturers.

Our experiments were designed to simulate as closely as possible the actual conditions under which this stereotaxic device operates during surgical applications. Obviously, there are differences between a plastic phantom and a human patient that will not allow all sources of error to be considered. As would be expected, our results show that the accuracy of the device decreased from the Plexiglas to the skull phantom and was slightly less accurate in our initial patient population. Clinical trials are currently under way to more fully validate the use of the arm with patients.

Several different considerations will affect how well the wand will operate. Comparison of the data from the various registration sets shows that the more widely dispersed the registration markers are in 3D space, the lower the average error. The facial registration markers were very nearly in the same plane, which explains the greater inaccuracy in this data set. The left lateral, right lateral, and back marker sets were more widely distributed, resulting in less error, while the global set, the most dispersed, had the least error. The median error for the facial registration set was 2.02 mm, versus 1.22 mm for the global registration set (Table 2). The 95th percentile value for the facial registration was 3.78, whereas the same value for the global registration set was 2.55 mm. The largest errors in the 95th percentile measurements were in the facial and back registration sets. This may be explained by the planar placement and the close proximity of the markers to each other, as discussed below.

Correlation analysis of the various registration sets suggests a very weak relationship between error and the distance of the tested point from the registration set. The trend is toward higher error at a greater distance. The range of error for a point at any given distance is large, however, thus providing only a general error prediction. Global registration is the exception. In this case, the trend is toward lower errors as the distance of the measured point from the registration set increases (ie, as the measured points move inward from the periphery of the head). This is a result of the same phenomenon that causes

higher error when planar registration sets are used. The transformations made to minimize the registration point error are all linear rigid body operations. Therefore, transformations made to points along the periphery of the data set cannot affect points within this boundary more than the peripheral registration points themselves. In other words, any scale-rotate operation affects the points farthest from the center of the data set the most (translations affect all points equally). If the error is constrained at these points, it should be minimized for the entire data set, assuming the coordinates for these points are entirely accurate. Registration transformations that constrain only points predominantly toward one side or area of the data set leave the points outside this region free to shift farther away from their corresponding locations (Fig 10). Thus, the more widespread the registration points, the higher the correlational accuracy between the actual anatomy and its reconstruction. In response to this observation, a new registration method is being evaluated that is dependent on the entire craniofacial contour.

Table 3 shows a comparison of our measured error for the combined data set with the results reported by Galloway et al. Their data listed in this Table are based on scanning parameters of 4-mm section thickness, similar to our data. Our combined data error is smaller by a factor of 1.06–2.00, in comparison with the accuracy of the framed stereotaxic units.

In general, errors will be approximately 2 mm with this frameless stereotaxic system, with 95% of the errors between 0 and 3.7 mm and maximum errors between 4 and 5 mm. The preliminary evaluation of the system in these initial patients revealed similar results, with an error range between 0.3 and 2.2 mm.

Although technically this system is a stereotaxic system, the differences between it and the more conventional systems now in use have important implications for the future. The comparable or better accuracy, plus the added flexibility of this system, promises an important advance over conventional framed stereotaxic units, not only improving the transfer of imaging information but also aiding surgical flexibility. Of equal importance is that the surgical field remains uncluttered.

Future Directions

To date, the majority of uses for tumor localization and resection delineation have been in neurosurgical and otolaryngologic cases. Several new areas, however, are being explored. Applications in craniofacial reconstruction that have been evaluated include using the system with the standard data to evaluate bone displacement and facial symmetry and using the reconstruction software before surgery to estimate and program into the computer the changes that are to be made during surgery. Efforts are also being made to use the system to identify biopsy sites and correlate these data with metabolic information from MR spectroscopy and positron emission tomography studies. The improved soft-tissue resolution of MR imaging and the ease of coregistration of several sequences obtainable in the same patient will increase the use of this digitized information for stereotaxic procedures.

Changes in the system hardware and software to enhance the usability and applicability of the system are also being planned. New surface-fitting algorithms that reduce the dependence on fiducial markers by fitting the data to facial and cranial contours have recently been implemented and will be evaluated in future publications. Work is also being performed to lessen the susceptibility of the system to head movements. Currently, the system is dependent on the head being rigidly fixed in reference to the mechanical arm to maintain accuracy throughout the surgical procedure. Methods being investigated to reduce or eliminate this problem include a mechanical "head follower," similar to the mechanical arm used for localization, and an ultrasonic position-sensing device that would be attached to the patient during registration. Both of these devices would be able to detect changes in head position and allow the computer to compensate. ■

Acknowledgments: We are grateful to Bruce Leggett, MSc, and Christopher Gabe, BSc, of I.S.G. Technologies for their technical support, to Richard Royall, PhD, for his help with the statistical analysis of our data, and to Mary McAllister for her editorial assistance.

References

1. Manaley MS, Mettlin C, Natazavan N, et al. National survey of patterns of care for brain-tumor patients. J Neurosurg 1989; 71:826–836.
2. Woolsley TD, Eldred CA. A summary report on the survey of intracranial neoplasms. Rockville, Md; Westat, 1977.
3. Natazavan N, Mettlin C, Murphy GP. Patterns of care surveys of the American College of Surgeons' Commission on Cancer. In: Mettlin C, Murphy GP, eds. Progressive cancer control: III. a regional approach. New York, NY: Liss, 1983; 187–199.
4. Dumas-Duport C, Kelly PJ. A histologic and cytologic method for the special definition of gliomas. Mayo Clin Proc 1987; 62:435–449.
5. Kelly PJ, Dumas-Duport C, Scheithauer BW, Kall BA, Kispert DB. Stereotactic histologic correlation of CT and MRI defined abnormalities in patients with glial neoplasms. Mayo Clin Proc 1987; 62:450–459.
6. Roberts DW, Strohbehn JW, Hatch JF, et al. A frameless stereotactic integration of CT imaging and the operating microscope. J Neurosurg 1986; 65:545–549.
7. Zinreich SJ, Kennedy DW, Long DM, Carson BS, Dufresne CR. 3D applications in neuroradiology. Hospimedica 1990; 8:29–32.
8. Zinreich SJ, Mattox DE, Kennedy DW, et al. 3D CT for cranial facial and laryngeal surgery. Laryngoscope 1988; 98:1212–1219.
9. Zinreich SJ, Dekel D, Leggett B, et al. Three-dimensional CT interactive "surgical localizer" for endoscopic sinus surgery and neurosurgery (abstr). Radiology 1990; 177(P):217.
10. Stuart A, Ord JK. Kendall's advanced theory of statistics. Vol 2. London, England: Oxford University Press, 1991; 776–785.
11. Galloway RC, Maciunas RJ, Latimer JW. The accuracies of four stereotactic frame systems: an independent assessment. Biomed Instrum Technol 1991; 25:457–460.
12. Ajmone-Marsan C, Abraham K. Considerations of the use of chronically implanted electrodes in seizure disorders. Confin Neurol 1960; 27:95–110.
13. Orville A, Smith JR, Clarke N. Central autonomic pathways: a study in functional neuroanatomy. J Comp Neurol 1964; 3:399–406.
14. Lunsford LD, Latchaw RE, Vries JK. Stereotactic implantation of deep brain electrodes using computed tomography. Neurosurgery 1983; 13:280–286.
15. Bosch DA. Indications for stereotactic biopsy in brain tumors. Acta Neurochir (Wien) 1980; 54:167–179.
16. Edner G. Stereotactic biopsy of intracranial space-occupying lesions. Acta Neurochir (Wien) 1981; 33:213–214.
17. Crain BJ, Bigner SH, Johnson WW. Fine needle aspiration biopsy of deep cerebrum: a comparison of normal and neoplastic morphology. Acta Cytol (Balt) 1983; 26:772–778.
18. Backland EO. Studies on craniopharyngiomas. III. Stereotactic treatment with intracystic yttrium-90. Acta Chir Scand 1973; 139:237–247.
19. Zamorano L, Dujovny M, Malik G, Yakar D, Mehta B. Multiplanar CT-guided stereotaxis and 1251 interstitial radiotherapy: image-guided tumor volume assessment, planning dosimetric calculation, stereotactic biopsy and implantation of removable catheters. Appl Neurophysiol 1987; 50:281–286.
20. Hildebolt CF, Vannier MW, Knapp RH. Validation study of skull three-dimensional computerized tomography measurements. Am J Phys Anthropol 1990; 82:283–294.
21. Galloway RL, Maciunas RJ. Stereotactic neurosurgery. Crit Rev Biomed Engl 1990; 18:181–205.